

Supplemental Information

Materials and Methods

Device Model - Geometry Validation

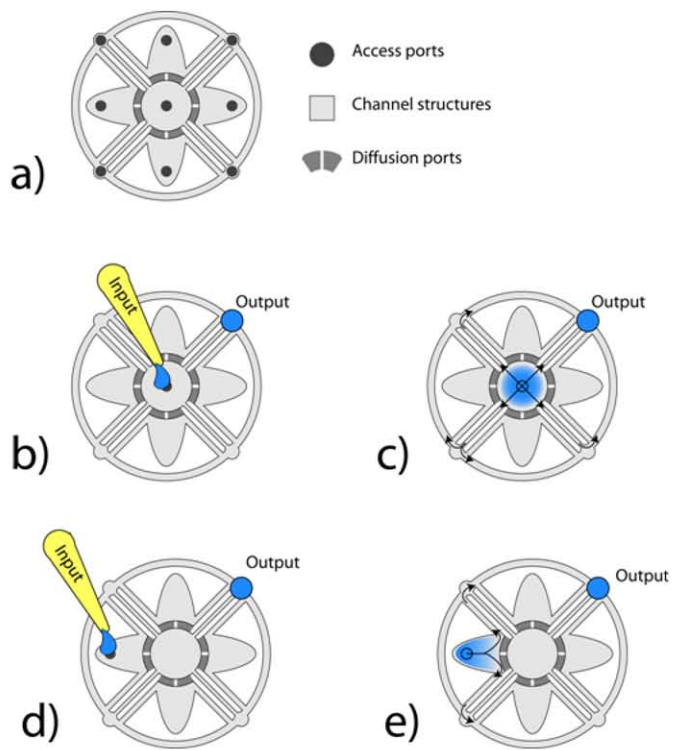
In order to model the diffusion ports of the device in 2-D, the diffusion ports had to be modeled as radial slits emanating from the center chamber and extending to the lobes. In the actual device, as shown in Fig 2 of the manuscript, the diffusion ports have a height that is 12-17 μm compared to the 250 μm height of the chambers. If the diffusion ports are to be modeled in 2-D this difference height must be reconciled as the diffusive flux through the diffusion ports is proportional to cross-sectional area yet, in 2-D, all depths into the page are assumed to be equal.

If the diffusion ports were to be 250 μm high (the same as the adjacent chambers), their cross-sectional area would be ~ 17 times greater than if they were made to be 12-17 μm high, therefore, if the top view dimensions of the diffusion ports are not altered for the 2-D simulation, the flux would be roughly 17 times too high. To remedy this, the diffusive flux through the diffusion ports in the 2-D simulations must be reduced by a factor of $\sim 1/17$ th. In steady-state simulations, this can be accomplished by assigning the diffusion coefficient, D , to be different in the diffusion ports as compared to the chambers. Since the diffusive flux is inversely proportional to D , the flux could be reduced appropriately by multiplying the diffusion coefficient by 17 in the diffusion port region only. However, this can only be done in steady-state simulations. This is because diffusion times scale differently with length, L , as compared to the effects of changes in D . This can be seen in the equation for the characteristic diffusion time of a solute over a distance L . The equation is, $t_d = L^2/(2D)$. Thus, in time-dependent solutions, one cannot simply alter the diffusion coefficient and achieve appropriate transient behavior of the model. Therefore, the diffusive flux must be reduced a different way.

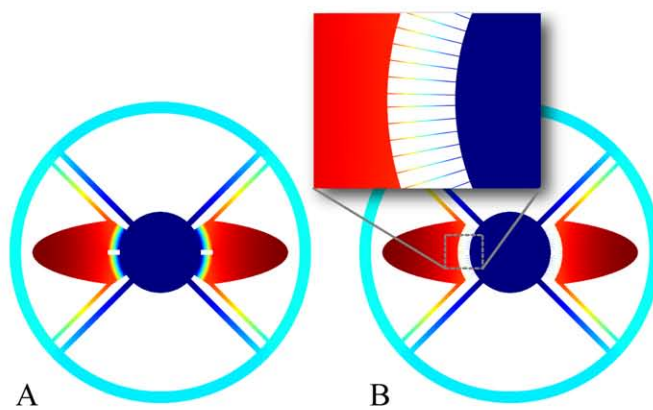
The diffusion flux was instead reduced by using diffusion slits that, in total, have a cross-sectional area of roughly $\sim 1/17$ th the original (see Supplemental figure 2B). The slits are not uniform in cross-section as they extend outward; instead, each side of a slit is formed by a line extending from the center of the center chamber creating a radially expanding slit to better mimic the gradient in the actual device. There are 20 slits per lobe in order to distribute the diffusing factor evenly as it leaves and enters chambers, mitigating uneven distribution that could arise from discretizing the diffusion ports. Since, the path length of diffusion is the same for the diffusion slits as for the original diffusion ports, the characteristic diffusion time is unaltered. By keeping the characteristic diffusion time the same, accurate transient behavior of the model is maintained. A comparison of the top views of the original device and altered device are shown in the Supplemental figure 2 A and B respectively, including a close-up view of the diffusion slits.

The accuracy and validity of the alteration in geometry can be tested by comparing results in a steady-state diffusion simulation. As mentioned earlier, in steady-state simulations, the diffusion port flux of geometry A can be altered by altering the diffusion coefficient to be $D/15$ in the region of the diffusion port only. In geometry B, only the dimensions of the diffusion slits are used to reduce flux. The modeling parameters used for the comparison were as follows. The lobes were set to a steady-state production of factor, Q [$\text{mol m}^{-3} \text{s}^{-1}$] and the concentration in the

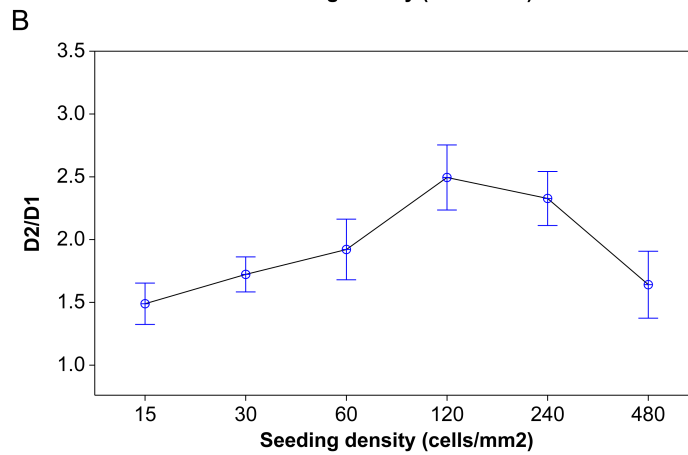
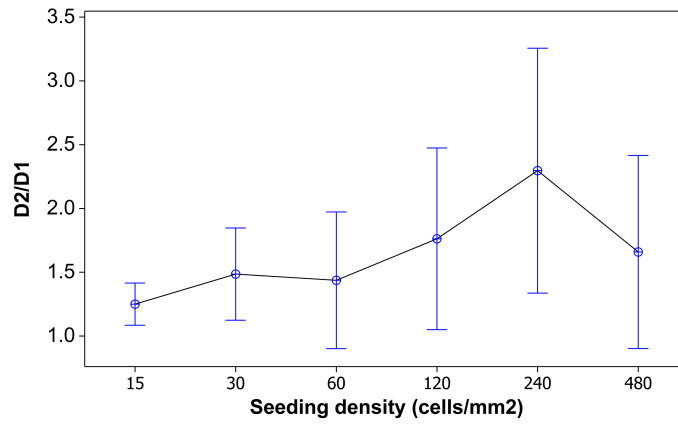
center chamber was set to 0. At steady-state, $\Delta C \propto (Q R)$, where ΔC is the change in concentration through the diffusion port and R is the diffusive resistance of the diffusion port. Since the simulation is for steady-state, we know that the flux to the center chamber is the same in both geometries. Therefore, if we take the ratio of the ΔC 's we can obtain the ratio of the diffusive resistances. When this is done, we find that the diffusive resistances of the diffusion ports in the two simulations agree to within 1.5%. Thus, the diffusion slits have achieved the goal of appropriately altering the flux through the diffusion ports while maintaining the accuracy of the model's transient behavior.



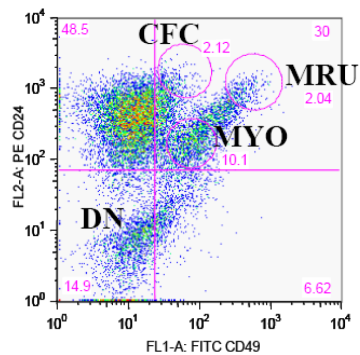
Supplemental Figure 1



Supplemental Figure 2



Supplemental Figure 3



Supplemental Figure 4

Supplemental figure 1. Schematic representation of the seeding process in a five well coculture microchannel. a) The structure has nine access ports, one for each of the five chambers and four for a peripheral output "track". The side chambers have input ports distal from the center and two channels branching from the inner end of the chamber leading to the output track. When an output drop is placed on one of the output ports, and a drop is delivered at the central chamber's input port (b) flow proceeds symmetrically towards all four exits from that chamber (c) filling that chambers with the input fluid. When a drop is delivered to one of the side chamber inputs (d) flow proceeds toward the center, fills the chamber up to the diffusion ports (e) and fluid exits through the side channels and flows toward the output track.

Supplemental figure 2. Comparison of geometry and steady state simulation results. Geometry A was modeled using a diffusion coefficient of $D/15$ in the region of the diffusion ports and D everywhere else. Geometry A utilized radially expanding diffusion slits to reduce flux between the lobes and center chambers by a factor of $1/15$ while maintaining the integrity of the transient behavior of the system. The steady state simulation set volumetric production constant in the lobes and concentration to 0 in the center chamber. The results indicate that the diffusive resistance between the lobes and center chamber for the two simulations is within 1.5% indicating that the diffusion slits reduced flux appropriately to model the actual change in cross-sectional area that occurs in the device used for experiments.

Supplemental figure 3. Effects of the seeding density on the growth of NMuMG cells (B) and MECs (A) cultured in microchannels (Figure 6A columns 3 and 9). NMuMG cells and MECs were seeded into Matrigel coated microchannels (A) with the same geometry to achieve 480, 240, 120, 60, 30 and 15 cells/mm² at the starting time point (Day 1 - D1). The growth rates within 24hrs were determined from Hoechst 33342 stained cultures from two plates (Day 1 and Day 2) by using the plate reader and a scanning epifluorescence microscope, $n = 6$. B) The growth rate (signal ratio of D2 to D1) and the confluency of the cultures were plotted against surface density at D1. The growth rate of NMuMG cells was seeding density dependent and the maximal population expansion was found at ~ 120 cells/mm²; C) The growth rate of MECs in the same setup was seeding density dependent, however the maximal growth rate were obtained with surface density ranging 100 \sim 300 cell/mm². ($p < 0.05$).

Supplemental figure 4. Representative fractions of MECs sorting in FACS experiments. There were 2.04 % of the MECs had the CD45⁻Ter119⁻CD31⁻CD49f^{hi}CD24^{med} phenotype (labeled with MRU) and 2.12 % of the MECs CD45⁻Ter119⁻CD31⁻CD49f^{low}CD24^{high} (CFC) and 10.1% of the MECs were CD45⁻Ter119⁻CD31⁻CD49f⁺CD24^{low/-} (MYO); there were also other populations with different expression level of CD49f and CD24, and the populations on the lower-left quadrant did not express CD49f or CD24 (DN).